東北大学機関リポジトリ
TOUR
Tohoku University Repository

Design, fabrication and evaluation of metal-matrix lightweight magnetostrictive fiber composites

著者	Zhenjun Yang, Kenya Nakajima, Lixin Jiang, Hiroki Kurita, Go Murasawa, Fumio Narita
journal or publication title	Materials & Design
volume	175
number	107803
page range	1-8
year	2019
URL	http://hdl.handle.net/10097/00129624

doi: 10.1016/j.matdes.2019.107803

Creative Commons : 表示 - 非営利 - 改変禁止
http://creativecommons.org/licenses/by-nc-nd/3.0/deed.ja

Materials and Design 175 (2019) 107803

Contents lists available at ScienceDirect

Materials and Design

journal homepage: www.elsevier.com/locate/matdes

Design, fabrication and evaluation of metal-matrix lightweight magnetostrictive fiber composites

Zhenjun Yang [a], Kenya Nakajima [a], Lixin Jiang [b], Hiroki Kurita [a], Go Murasawa [b], Fumio Narita [a,*]

[a] Department of Materials Processing, Graduate School of Engineering, Tohoku University, Sendai 980-8579, Japan
[b] Department of Polymer Science and Engineering, Yamagata University, 4-3-16 Jonan, Yonezawa 992-8510, Yamagata, Japan

GRAPHICAL ABSTRACT

A class of 1-3 lightweight metal-matrix FeCo/Al composites with promising capacity in high-temperature application was fabricated. This series of FeCo/Al composites exhibit the excellent energy-harvesting performance even at a relatively low stress-rate and bias magnetic field.

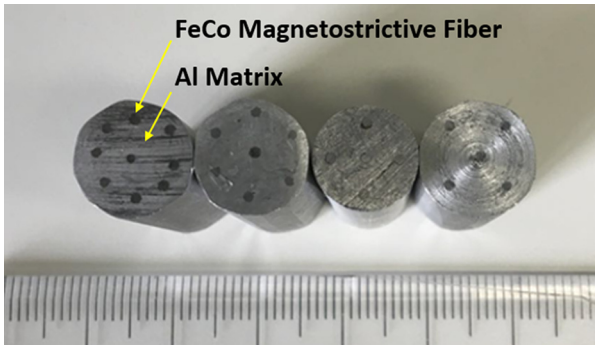

ARTICLE INFO

Article history:
Received 20 February 2019
Received in revised form 9 April 2019
Accepted 17 April 2019
Available online 23 April 2019

Keywords:
Metal-matrix composite
Iron cobalt
Inverse magnetostrictive effect
Lightweight devices

ABSTRACT

A class of lightweight FeCo/AlSi magnetostrictive composites was prepared in this study to explore the feasibility for 1-3 metal-matrix magnetostrictive materials for serving as sensors, actuators and energy harvesters. The FeCo fibers were inset into the AlSi metal liquid and then the composites were solidified at a protective atmosphere. The microstructural observations for these FeCo/AlSi composites illustrate the presence of the element diffusion and the disappearance of the cold-rolled preferred orientation. The refined microstructure was obtained during solidification and then further improved the magnetostrictive properties of the FeCo/AlSi composites. A zigzag interface with well transfer in stress and strain between the FeCo fiber and AlSi matrix existed through both physical and chemical bonding. There are two different experimental groups in this work. One group is aimed to evaluate the effect of the diameter of the FeCo/AlSi composite on the output voltage under compression. Another group with different numbers of the FeCo fibers is employed for analyzing the effect of the volume fraction of the FeCo fiber on the output performance. The results exhibit that a smaller diameter for the lightweight 1-3 FeCo/AlSi composite contributes to exciting a greater output voltage. Furthermore, the output voltage is proportional to the number of the FeCo fiber. An optimal resistive load of 500 Ω for this harvesting setup is obtained. Theoretical analysis through a magneto-mechanical coupling model for the FeCo/AlSi composites was conducted for accurately predicting the practical output performance.

© 2019 The Authors. Published by Elsevier Ltd. This is an open access article under the CC BY-NC-ND license (http://creativecommons.org/licenses/by-nc-nd/4.0/).

* Corresponding author.
E-mail address: narita@material.tohoku.ac.jp (F. Narita).

https://doi.org/10.1016/j.matdes.2019.107803
0264-1275/© 2019 The Authors. Published by Elsevier Ltd. This is an open access article under the CC BY-NC-ND license (http://creativecommons.org/licenses/by-nc-nd/4.0/).

1. Introduction

Magnetostrictive materials have been widely studied in recent years as multifunctional components in sensors, actuators and energy harvesters. This series of materials provide a promising potential not only in sensitive electro-mechanical conversion but also in self-powered microsystems powering lots of micro-units in the Internet of Things (IoT) [1–4]. In particular, these relevant applications for magnetostrictive materials have been attracting increasing consideration because of the requirements of miniaturization and complication for power-supporting components [5–8].

Several main magnetostrictive materials have been examined due to their excellent magnetostrictive properties. Terfenol-D is thought to be widely applied in consideration of its high magnetostriction. Some researchers [9,10] employed this material for fabricating a class of sensors, actuators, etc. However, the natural brittleness of Terfenol-D constrains its further application to a great extent [11,12]. Improving the issue has become an imminent challenge. Although fabricating the corresponding composites has the capability of improving its brittle property, it is always at the expense of reducing whole magnetostrictive properties of the composites. Moreover, the final results often indicated that there is only a limited improvement in brittleness. On the other hand, Galfenol alloy, referred to FeGa alloy, exhibiting certain metal properties and great magnetostriction has been recognized as a possible substitute for brittle Terfenol-D. Nevertheless, sophisticated processing for Galfenol alloys is required in order to obtain appropriate microstructures with great magnetostrictive properties and sizes. Besides, combing with the relatively high costs of the raw materials, this material is generally difficult to realize the widespread industrialization at present [13,14]. Considering these aforementioned reasons, some other materials [15–18] have been also identified as potential substitutive candidates, such as FeCo, amorphous materials, etc. In particular, FeCo alloy exhibits comparable magnetostrictive properties to Galfenol alloy and excellent processing merits. According to the recent work [19], a series of clad FeCo plate cantilevers (FeCo/Ni and FeCo/Fe, etc.) have been fabricated, which already demonstrated its promising ability for serving as an effective magnetostrictive material. Furthermore, our other research [20] also manifested that a reasonable shape design is capable of enhancing the localized stress concentration and strain transfer, further leading to a significant increase in the output performance.

Various magnetostrictive materials with different specific properties have the benefit of satisfying different in-service requirements. However, given the feature of magnetic transformation, there is still a problem that how to maintain relatively high magnetostrictive properties and thermal stability at an elevated temperature for a magnetostrictive material. It is commonly believed that a high Curie temperature is crucial to maintain the thermal properties for a magnetostrictive material. However, the Curie temperatures for the magnetostrictive materials Terfenol-D and Galfenol are only 380 and 680 °C, respectively [21]. It is therefore necessary to identify a promising candidate that is capable of being applied at an elevated temperature. On the other hand, a great of works with respect to magnetostrictive composites were focused on the junction between polymers and magnetostrictive materials. It restricts the further application for magnetostrictive composite in a way because of natural demerits of polymers, such as weak heat-resistance and mechanical properties, etc. Although metal-matrix magnetostrictive composites were also studied [19,21], most of work were generally aimed to fabricate a class of multilayer magnetostrictive composites.

In this study, we aim to propose an approach for fabricating a promisingly 1-3 metal-matrix magnetostrictive composite that is of the excellent magneto-mechanical conversion and the feasibility in industrialization. Therefore, easy-producible FeCo alloy was employed in view of its high Curie temperature (900 °C) that possesses excellent thermal stability as well as high magnetization at a relatively high temperature. Besides, a heat-resistant lightweight AlSi matrix is utilized for providing good stress and strain transfer stemming from the applied loading even at a high temperature. As a consequence, a class of 1-3 metal-matrix FeCo/AlSi magnetostrictive composites that exhibits both great magnetostrictive and mechanical properties was proposed, which is able to be served as feasible high-temperature sensors, actuators and energy harvesters.

2. Experiment

It has been well demonstrated that FeCo alloys with relatively good magnetostrictive properties are able to be applied in sensors and energy harvesters. To prepare the FeCo fiber, first of all, the raw materials were melted in a furnace. Following, the forging process was employed to shape the melted metals into the crude ingots. After that, the ingots underwent hot- and cold-rolling, and then through cold drawn to obtain the FeCo fibers with a diameter of 1 mm. Here, a class of FeCo/AlSi composites was fabricated in this study to examine the variations of energy conversion in response to the applied loadings. A kind of AlSi alloy, referred to AC3A (Japanese industrial standards, see Table 1), was employed to be the matrix. In more detail, the AlSi ingots were melted at 700 °C. After that, the FeCo fibers were embedded into the AlSi metal liquid until the composite completely solidified at an Ar protective atmosphere. Two different groups were prepared for analyzing the effects of the number of FeCo fiber and the diameter on magnetostrictive properties and energy harvesting performance for this class of composites. The first group of the FeCo/AlSi composites with a diameter of 12 mm was divided into three subgroups with the different numbers of FeCo fibers of 5, 7 and 9, respectively. On the other hand, the second group with the same number of FeCo fiber (i.e., 5 FeCo fibers) was classified into two subgroups with the diameters of 10 and 12 mm for the FeCo/AlSi composites. Here, it must be emphasized that the FeCo fibers treated by cold-rolled treatment were in the same diameter of 1 mm. Furthermore, all of those samples had an identical length of approximately 25 mm. The schematic and photographs for this series of FeCo/AlSi composites are shown in Fig. 1. The volume fraction v^f, cross-sectional area A^f of the FeCo fibers within the whole FeCo/AlSi composite, and fiber's diameter and number are listed in Table 2, where the superscript *f* denotes the FeCo fiber.

Uniaxial cyclic compression tests were carried out for every sample at five times as shown in Fig. 2. Each step includes a loaded and unloaded processes with the same magnitude of the maximum stress $\sigma_{max} = P_{max}/A$, where P_{max} denotes the maximum stress and A denotes the cross-sectional area of the composite. The compressing force was applied at constant crosshead velocities of $d\delta/dt = 0.25$, 0.5, 0.75, 1.0 and 2.0 mm/s, where δ denotes the crosshead displacement and t denotes the time. Two different bias magnetic fields B_0 of 33 and 75 mT were introduced to magnetize the FeCo/AlSi composites. A pickup coil with 2500 turns that connected with a data logger was used to measure the output voltage V_{out}. Besides, considering the procedure of solidification for those FeCo/AlSi composites, the corresponding element distribution and the microstructures were also determined through the energy-dispersive detector (EDS), scanning electron microscopy (SEM) and electron backscatter diffraction (EBSD), respectively.

3. Theoretical analysis

To analyze the magnetostrictive properties, the theoretical calculation is necessary for explaining and manifesting the energy-conversion mechanism quantitatively. According to the feature of the

Table 1
Composition of the AlSi alloy.

Elements	Al	Si	Cu	Mg	Zn	Fe	Mn
Wt%	>80.00	10.00	0.25	0.15	0.30	0.8	0.35

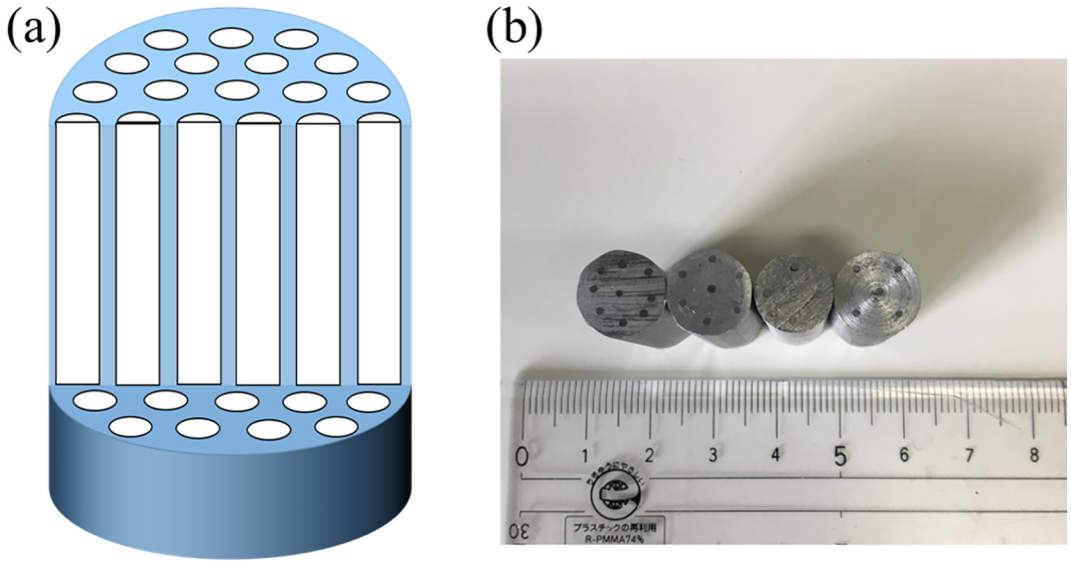

Fig. 1. (a) Schematic and (b) photograph of the FeCo/AlSi composite.

magnetostrictive principle [21,22], the constitutive equations can be given as below

$$\varepsilon = s\sigma + d'H, \tag{1}$$

$$B = d'\sigma + \mu H, \tag{2}$$

where σ and ε represent the stress and strain, and B and H are the magnetic induction and magnetic field intensity, respectively. The symbols of s, $d'$and μ denote the elastic compliance, magnetoelastic constant and magnetic permeability, respectively. The magnetoelastic constant d' could be calculated by

$$d' = d + (m + r\sigma_0)H, \tag{3}$$

where d is the piezo-magnetic constant, m is the constant that physically denotes the magnetostrictive strain produced by per unit external magnetic field and r is the constant that physically refers to the coupling magnetostrictive strain produced by per unit external magnetic field under per unit internal stress [23]. Here, the effect of residual stress was taken into account. Thus, σ_0 denotes the residual stress within the FeCo fiber. The relevant residual thermal stress can be calculated through three-dimensional finite element analysis (FEA), which was shown in Appendix A.

Let us now consider the Rectangular Cartesian coordinates x_i (O-x_1, x_2, x_3). It was assumed that the easy axis to be magnetized for the FeCo fiber is along the x_3-direction (i.e. the direction of length) according to relative experimental results as shown in Appendix B. On the other hand, when the length of a magnetostrictive fiber is far greater than its diameter, and the bias magnetic field is also along the x_3-direction, the longitudinal magnetostrictive deformation mode (33) is dominant. Hence, during compression along the x_3-direction, the x_3-component of the magnetic field intensity vector is almost responsible for the whole variation of the magnetoelastic constant. As a result, the three-dimensional model was simplified as a one-dimensional model, namely, only along the x_3-direction. Therefore, the constitutive Eqs. (1) and (2) could be substituted by the following equations

$$\varepsilon_{33}^f = s_{33}^f\sigma_{33}^f + d_{33}^f + \left(m + r\sigma_0\right)H_3^f\Big\}H_3^f, \tag{4}$$

$$B_3^f = \left\{d_{33}^f + (m + r\sigma_0)H_3^f\right\}\sigma_{33}^f + \mu_{33}^f H_3^f, \tag{5}$$

where ε_{33}^f, σ_{33}^f are the components of strain and stress tensor, B_3^f, H_3^f are the components of magnetic induction and magnetic field intensity

Table 2
Relevant parameters of FeCo/AlSi composites.

Specimen	v^f	A^f (mm^2)	Diameter (mm)	Fiber's number
D10F5[a]	0.0500	3.925	10	5
D12F5	0.0347	3.925	12	5
D12F7	0.0486	5.495	12	7
D12F9	0.0625	7.065	12	9

[a] Note: D denotes the diameter of composite and F denotes the number of FeCo fiber.

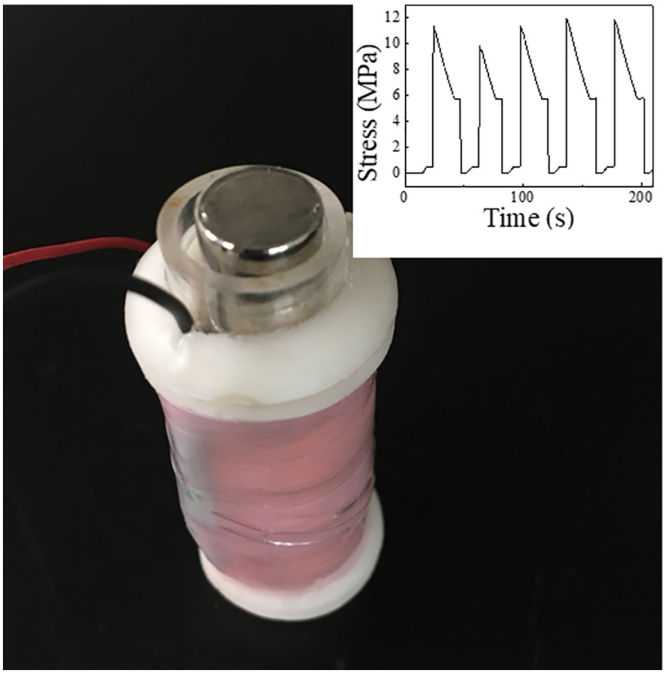

Fig. 2. Physical assembly for the energy-harvesting setup under compression and the upper-right inset showing the five-time cycles.

Table 3
Some parameters of the FeCo fiber and AlSi matrix.

s_{33}^m ($\times 10^{-12}$ m^2/N)	s_{33}^f ($\times 10^{-12}$ m^2/N)	d_{33}^f ($\times 10^{-9}$ m/A)	m ($\times 10^{-12}$ m^2/A^2)	μ_{33}^f ($\times 10^{-6}$H/m)
13	5.5	0.125	0.0123	37.7

vectors, and $s_{33}^f, d_{33}^f \mu_{33}^f$ are the elastic compliance, piezo-magnetic constant and magnetic permeability, respectively. The calculating parameters for the FeCo fiber [24] and AlSi matrix are listed in Table 3. In general, it is reasonably believed that the induced magnetic field intensity resulting from the inverse magnetostrictive effect is far smaller as compared to the bias magnetic field $H_0 = B_0/\mu_0$ (where $\mu_0 = 1.26 \times 10^{-6}$H/m is the magnetic permeability of free space). In this case, the Eqs. (4) and (5) could be further simplified as below

$$\varepsilon_{33}^f = s_{33}^f \sigma_{33}^f + d_{33}^f \left(\frac{B_0}{\mu_{33}^f}\right) + (m + r\sigma_0)\left(\frac{B_0}{\mu_{33}^f}\right)^2, \tag{6}$$

$$B_3^f = \mathrm{d}_{33}^f \sigma_{33}^f + (m + r\sigma_0)\left(\frac{B_0}{\mu_{33}^f}\right)\sigma_{33}^f + B_0, \tag{7}$$

The strain tensor component ε_{33}^m and magnetic induction vector component B_3^m for the AlSi matrix are given by

$$\varepsilon_{33}^m = s_{33}^m \sigma_{33}^m, B_3^m = \mu_0 H_3^m, \tag{8}$$

where s_{33}^m are the elastic compliance for the AlSi matrix and the superscript m denotes the AlSi matrix. Here, it was assumed that the perfect bonding between the FeCo fiber and AlSi matrix impose, that is, $\varepsilon_{33}^f = \varepsilon_{33}^m$.

The representative volume element was modeled as a single cylindrical FeCo fiber bonded within a cylinder of the AlSi matrix. The relevant volume fractions for every sample are also listed in Table 2. Because of the transverse isotropy of the representative volume element, the components of the stress tensors for the FeCo and AlSi matrix are uniform. The average stress σ_{33}^0 is therefore can be expressed by

$$\sigma_{33}^0 = \sigma_{33}^f v^f + \sigma_{33}^m \left(1 - v^f\right), \tag{9}$$

This σ_{33}^0 is equivalent to the stress imposed by the loading on the composite cylinder. The final output voltage of each composite is therefore calculated which can be shown as the following equation:

$$V_{\text{out}} = -NA^f \frac{dB_3^f}{dt} = -NA^f \frac{s_{33}^m}{s_{33}^m v^f + s_{33}^f (1 - v^f)} \left\{ d_{33}^f + \frac{(m + r\sigma_0)}{\mu_{33}^f} B_0 \right\} \frac{d\sigma_{33}^0}{dt}, \tag{10}$$

where N is the number of the pickup coil.

4. Results and discussion

Because the FeCo/AlSi composites were fabricated at a high temperature, analyzing the microstructure of these composites, especially around the interface between the FeCo fiber and AlSi matrix, is necessary. Fig. 3(a) shows the specific details upon the interfacial circumstance. The presence of element diffusion is obvious around the interface (shown by the white dashed line) depending upon the color contrast. It suggests that the chemical bonding is existed around the interface. Furthermore, the EDS analysis also indicates that the element diffusion certainly exists around the interface, especially for the Al element, as shown in Fig. 3(b). Besides, a zigzag boundary along the interface also reveals the presence of good physical bonding. As described above, the interface between the FeCo fiber and AlSi matrix exhibits relatively excellent bonding strength. As a result, it has the benefit of the stress or strain transformation through the interface, which plays an important role in magneto-mechanical energy conversion. Fig. 4 shows the EBSD diagrams of the FeCo fiber. The microstructure of the FeCo fiber after the thermal treatment (i.e., the solidification of the AlSi metal liquid) shows the different microstructural features in comparison to that of the FeCo fiber before the thermal treatment. In addition, the microstructure of the cold-rolled FeCo fiber is of the preferred orientation along the cold-rolling direction (see Fig. 4(a)). The EBSD diagram reveals that the red ribbon-like microstructure along the ⟨001⟩ direction is dominant for the cold-rolled FeCo fiber. However, after the thermal treatment, the FeCo fiber consists of the considerable equiaxed grains, namely, the aforementioned preferred orientation disappears in Fig. 4 (b). There is no existence of the rolled features in the microstructure even along the rolling directing. On the other hand, the domain rotation and wall movement are directly attributed to the microstructure in a way. Hence, the equiaxed grain for the FeCo fiber during compression is obviously susceptible to excite the variation of the magnetic induction as compared to the cold-rolled microstructure when the bias magnetic

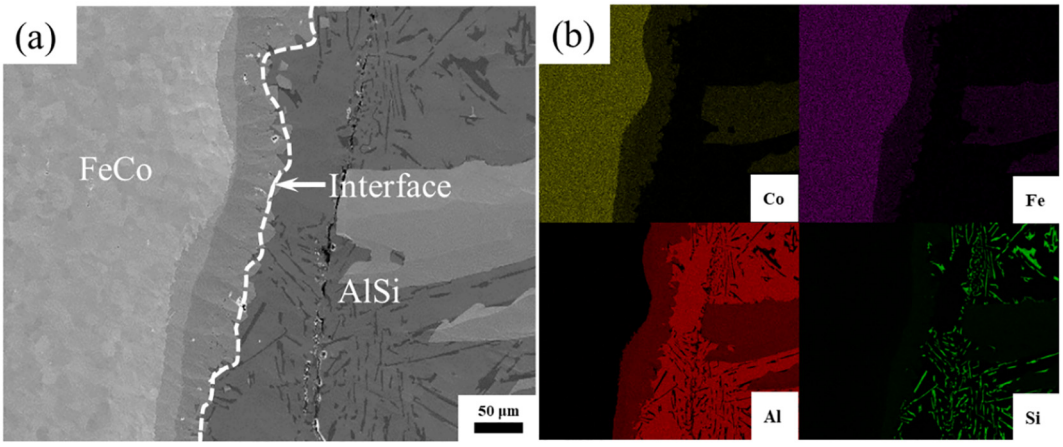

Fig. 3. (a) Microstructure and (b) element distribution around the interface of the FeCo/AlSi composite.

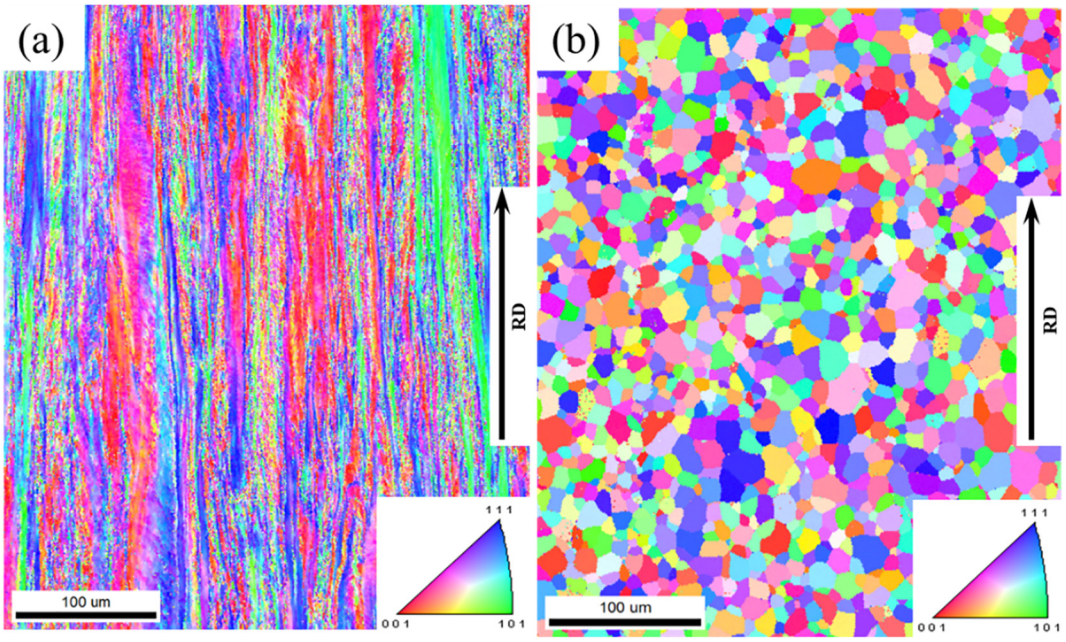

Fig. 4. EBSD diagrams showing the differences of the microstructure for the FeCo fibers before (a) and after (b) thermal treatment; RD denotes the cold-rolling direction.

field is completely accordance with the length direction for the FeCo fiber.

To evaluate the harvesting performance for the FeCo/AlSi composites, the output voltage V_{out} versus crosshead displacement velocity $d\delta/dt$ of the FeCo/AlSi composites with different diameters under a constant bias magnetic field of $B_0 = 75$ mT are shown in Fig. 5. Observing every single sample indicates that the output voltage is clearly proportional to the crosshead displacement velocity, that is, the stress rate. Namely, a higher velocity leads to a relatively higher stress rate, giving rise to the larger localized strain rate around the FeCo fibers. Therefore, there is an upward tendency for the output voltages resulting from the variations of magnetic induction with the increasing crosshead displacement velocity, while the relevant variation is sensitive to the applied loading. Besides, this comparison in Fig. 5 (D denotes the diameter of the FeCo/AlSi composite and F denotes the number of the FeCo fibers) also indicates that the output voltage of D10F5 is greater than that of D12F5, which manifests that the output voltage is certainly related to the stress rate on the cross-section in response to the applied loading. On the other hand, Fig. 5 also illustrates that the output voltage is proportional to the number of the FeCo fiber, referred to the volume fraction. Here, there is an interesting phenomenon that the increments of voltage for different fiber volumes are not completely consistent with the increase of volume fraction. Obviously, D12F9 exhibits a far greater increment in the output voltage. The reason is related to the stress distribution or strain transfer. In more detail, a larger FeCo fiber volume has the benefit of providing more magnetic induction variation and then being conversed to more output voltage. Moreover, a more dispersed distribution for the FeCo fiber with a larger volume fraction is inevitable to generate larger-scale stress concentration around the interface between the FeCo fiber and AlSi matrix owing to the different elastic modulus for each other. It is concluded that the superposition with respect to

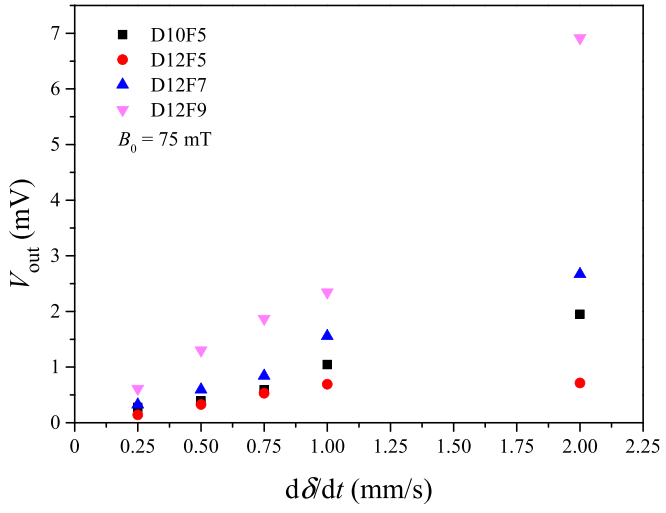

Fig. 5. Comparison of the output voltages for various FeCo/AlSi composites with different diameters under a bias magnetic field of 75 mT.

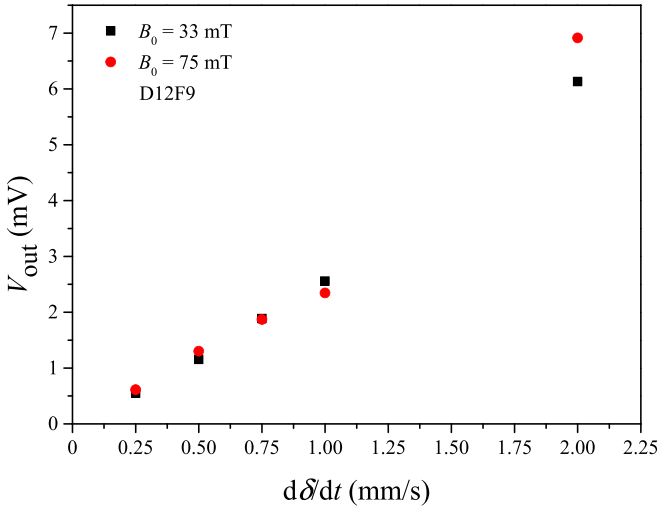

Fig. 6. Comparison of the output voltage for the FeCo/AlSi composite (D12F9) under different bias magnetic fields.

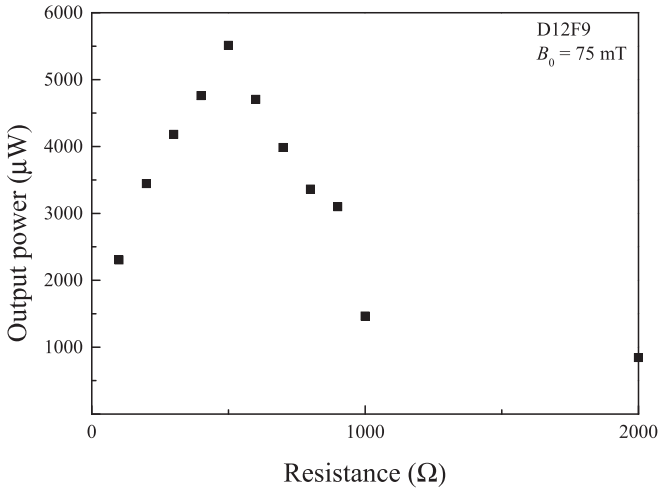

Fig. 7. Output power for the FeCo/AlSi composite (D12F9) with differing resistive loads at a constant crosshead displacement velocity of 1 mm/s.

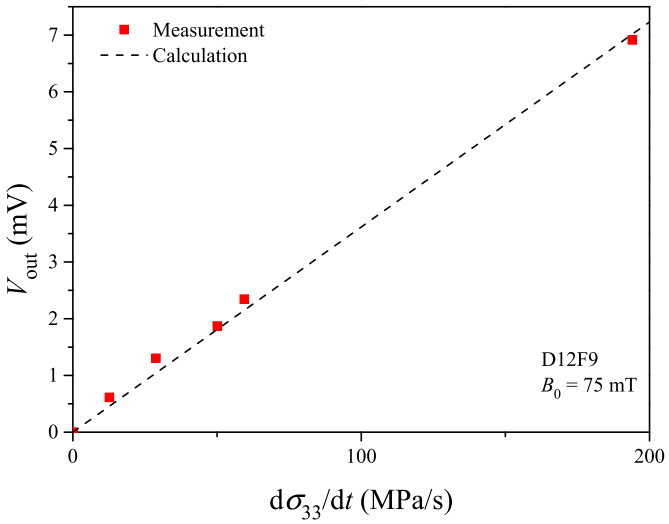

Fig. 8. Comparison of the output voltages between the calculation and measurement.

the aforementioned effects is responsible for the uneven increase in the output voltage with the increasing volume fraction for the FeCo fiber.

Another experimental group reveals the effects of the bias magnetic field on the output voltage. Fig. 6 shows the output voltage V_{out} versus crosshead displacement velocity $d\delta/dt$ of the FeCo/AlSi composite D12F9 under a constant bias magnetic field of $B_0 = 33$ and 75 mT. It is clear that the output voltage for the FeCo/AlSi composite shows a slight decrease under a relatively lower bias magnetic field of $B_0 = 33$ mT in comparison to that under $B_0 = 75$ mT. In particular, the variation of the output voltage is more significant at a relatively high crosshead displacement velocity. This phenomenon is generally attributed to the high saturated magnetization for the FeCo fiber. A larger applied loading, in a way, is able to be recognized as a larger bias magnetic field to drive the domain rotation or the movement of domain wall. Overall, it is clearly clarified that this material exhibits a promising ability in energy harvesting even at a relatively low bias magnetic field.

The measured output power for the FeCo/AlSi composite D12F9 at differing resistive loads and a constant crosshead displacement velocity of $d\delta/dt = 1$ mm/s was measured, and shown in Fig. 7. The results indicate that the harvesting setup has an optimal resistive load of approximately 500 Ω. Indeed, the optimal resistive load is directly associated with the pickup coil. Except for that, it cannot be ignored that this class of FeCo/AlSi composite has a relatively broad range in energy-harvesting applications.

The measured and calculated output voltages of the FeCo/AlSi composite D12F9 were compared. Fig. 8 illustrates that the calculated results almost completely coincide with experimental measurement. Here, according to Eq. (10), a residual stress of approximately 0.02 MPa within the FeCo fibers have been considered and the corresponding constant r is about 3×10^{-17} m^2 A^{-2} Pa^{-1}. In the case of the comparison, stress-rate $d\sigma_{33}^0/dt$ is employed to evaluate the output performance. In particular, the calculated results are proportional to the stress-rate in terms of the aforementioned theoretical analysis. The dashed line in Fig. 8 therefore shows a linear correlation with respect to the stress-rate. On the other hand, although there is a slight fluctuation in the output voltage of measurement as compared to the calculation curve, this phenomenon is able to be omitted in consideration of the error of physical assembly. As a consequence, this comparison is also well demonstrated that the theoretical calculation is capable of predicting the accurate output performance of FeCo/AlSi composite in this work.

5. Conclusions

A class of 1-3 lightweight metal-matrix FeCo/AlSi composites with promising capacity in high-temperature application was fabricated in this study. The corresponding microstructure and harvesting performance were systematically examined. The final results indicate that the process of solidification leads to the element diffusion and the disappearance of the cold-rolled feature. These changes have the benefit of improving output performance of the FeCo/AlSi composites. Besides, the output voltage is proportional to the crosshead displacement velocity that is related to the stress rate. Moreover, this series of FeCo/AlSi composites exhibit the excellent energy-harvesting performance even at a relatively low stress-rate and bias magnetic field. Besides, this harvesting setup shows an optimal resistive load of 500 Ω and a relatively broad applying range. Eventually, the comparison between the practical measurement and calculation manifests that the theoretical calculation is able to predict the output performance of the FeCo/AlSi composite. In a conclusion, given the relatively great high-temperature properties of these two materials (FeCo and AlSi), this work proposes a feasible exploration on fabricating a lightweight magnetostrictive composite that are potentially applied in sensors or energy harvesters especially at a relatively high temperature.

Contributions

Z.J. Yang is responsible for the performance measurement, calculation, FEA simulation, data analysis and writing the manuscript. K. Nakajima and H. Kurita help operate the apparatus and revise the manuscript. L.X. Jiang and G. Murasawa prepared the samples. F. Narita edited the manuscript and supervised the whole study.

Appendix A

Here, the details of how to predict the residual stress σ_0 of the sample are presented. A three-dimensional FEA is carried out for calculating the residual thermal stress within the FeCo fiber without magnetostrictive effect due to the change of temperature T, in view of that the presence of residual stress generally has an effect on domain rotation and/or wall movement. In order to coincide with the practical experiment, the simulation procedure is classified into three processes: (1) the FeCo/AlSi composite is heated from room temperature (20 °C) to 700 °C; (2) the sample is then cooled to 700 °C; and (3) unload the pressure of protective atmosphere (0.4 MPa). Here, a simplified model with an identical volume fraction of the specimens is considered as shown in Fig. A1, which exhibits a single FeCo fiber embedded in the AlSi matrix.

The constitutive equation can be expressed as

$$\begin{Bmatrix} \varepsilon_{11}^j \\ \varepsilon_{22}^j \\ \varepsilon_{33}^j \\ 2\varepsilon_{23}^j \\ 2\varepsilon_{31}^j \\ 2\varepsilon_{12}^j \end{Bmatrix} = \begin{bmatrix} s_{11}^j & s_{12}^j & s_{13}^j & 0 & 0 & 0 \\ s_{12}^j & s_{11}^j & s_{13}^j & 0 & 0 & 0 \\ s_{13}^j & s_{13}^j & s_{33}^j & 0 & 0 & 0 \\ 0 & 0 & 0 & s_{44}^j & 0 & 0 \\ 0 & 0 & 0 & 0 & s_{44}^j & 0 \\ 0 & 0 & 0 & 0 & 0 & s_{66}^j \end{bmatrix} \begin{Bmatrix} \sigma_{11}^j \\ \sigma_{22}^j \\ \sigma_{33}^j \\ \sigma_{23}^j \\ \sigma_{31}^j \\ \sigma_{12}^j \end{Bmatrix} + \begin{Bmatrix} \alpha^j \\ \alpha^j \\ \alpha^j \\ 0 \\ 0 \\ 0 \end{Bmatrix} \theta \quad (j = \mathrm{f}, \mathrm{m}) \tag{A.1}$$

where $\theta = T - T_R$ is the temperature change for the stress-free reference temperature T_R, and α^j $(j = \mathrm{f}, \mathrm{m})$ is the coefficient of thermal expansion, and $s_{11}^j, s_{12}^j, s_{13}^j, s_{44}^j, s_{66}^j$ are the elastic compliance. The detailed parameters for these two materials (i.e., FeCo and AlSi) are shown in Table A1.

Table A1
Relevant calculation parameters of the FeCo fiber and AlSi matrix.

Materials	Elastic compliance ($\times 10^{-12}$ m^2/N)						Coefficient of thermal expansion α (10^{-6}/K)
	s_{11}	s_{33}	s_{44}	s_{66}	s_{12}	s_{13}	
FeCo	5.5	5.5	14.3	14.3	−1.65	−1.65	11.9
AlSi	13	13	33.8	33.8	−3.9	−3.9	23.9

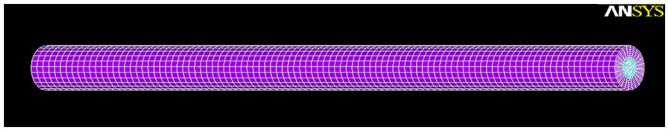

Fig. A1. Three-dimensional FEA model for the FeCo/AlSi composite.

Appendix B

To evaluate the easy axis to be magnetized for the FeCo fiber with polycrystallinity, the demagnetization is necessary to be considered because of the effect of geometric anisotropy. In general, the vital affecting factor, referred to demagnetization factor N_D, is a geometry-sensitive parameter. When the dimension of the FeCo fiber parallel to the magnetization is far greater than the vertical dimension, the effect of demagnetization is able to be omitted. In contrast, if the effect of demagnetization is present, the efficiency for magneto-mechanical energy conversion will reduce significantly stemming from the reduction of magnitude on the magnetic induction for the FeCo fiber, which is attributed to the cancellation between the magnetization and demagnetization. The aforementioned results have been well demonstrated in Fig. B1. Here, all data of the magnetostriction are measured along the direction of the bias magnetic field. It reveals that the magnetostriction of the FeCo fiber along the longitudinal direction (i.e. the fiber's long axis) is far greater than that along the direction vertical to the fiber's long axis. Moreover, according to the slopes of these curves, it also indicates that the piezomagnetic constant along the direction of the fiber's long axis is analogously greater than that along the direction vertical to the fiber's long axis. Namely, based on the constitute equations, the energy harvesting performance of the FeCo/AlSi composite will undergo a further decline when the magnetization direction is not parallel to the fiber's long axis.

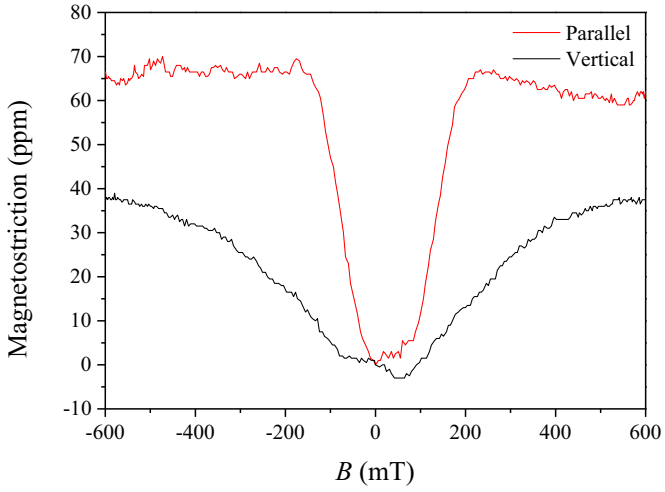

Fig. B1. Magnetostriction of the FeCo fiber with a diameter of 1 mm along the directions parallel and vertical to the fiber's long axis.

References

[1] Q. Zhang, Q.J. Liang, Z. Zhang, Z. Kang, Q.L. Liao, Y. Ding, M.Y. Ma, F.F. Gao, X. Zhao, Y. Zhang, Electromagnetic shielding hybrid nanogenerator for health monitoring and protection, Adv. Funct. Mater. 28 (2018) 1703801.

[2] H. Yoon, M. Kim, C.S. Park, B.D. Youn, Time-varying output performances of piezoelectric vibration energy harvesting under nonstationary random vibrations, Smart Mater. Struct. 27 (2018), 015004.

[3] D. Singh, A. Choudhary, A. Garg, Flexible and robust piezoelectric polymer nanocomposites based energy harvesters, Acs Appl. Mater. Inter. 10 (2018) 2793–2800.

[4] S.M. Na, J.J. Park, S. Lee, S.Y. Jeong, A.B. Flatau, Magnetic and structural anisotropic properties of magnetostrictive Fe-Ga flake particles and their epoxy-bonded composites, Mater. Lett. 213 (2018) 326–330.

[5] S.A. Sheikholeslami, M.M. Aghdam, E. Zappino, E. Carrera, Application of refined beam elements to the coupled-field analysis of magnetostrictive microbeams, Compos. Part B-Eng. 115 (2017) 14–20.

[6] C.D. Pham, J. Chang, M.A. Zurbuchen, J.P. Chang, Magnetic properties of CoFe2O4 thin films synthesized by radical enhanced atomic layer deposition, Acs Appl. Mater. Inter. 9 (2017) 36980–36988.

[7] L. Jin, W.L. Deng, Y.C. Su, Z. Xu, H. Meng, B. Wang, H.P. Zhang, B.B. Zhang, L. Zhang, X.B. Xiao, M.H. Zhu, W.Q. Yang, Self-powered wireless smart sensor based on maglev porous nanogenerator for train monitoring system, Nano Energy 38 (2017) 185–192.

[8] M.A.P. Mahmud, N. Huda, S.H. Farjana, M. Asadnia, C. Lang, Recent advances in nanogenerator-driven self-powered implantable biomedical devices, Adv. Energy Mater. 8 (2018), 1701210.

[9] A. Yoffe, D. Shilo, The magneto-mechanical response of magnetostrictive composites for stress sensing applications, Smart Mater. Struct. 26 (2017), 065007.

[10] Z.X. Deng, Explicit and efficient discrete energy-averaged model for Terfenol-D, J. Appl. Phys. 122 (2017), 043901.

[11] M. Colussi, F. Berto, K. Mori, F. Narita, Fracture behavior of cracked giant magnetostrictive materials in three-point bending under magnetic fields: strain energy density criterion, Adv. Energy Mater. 18 (2016) 2063–2069.

[12] M. Peron, K. Katabira, L.M. Viespoli, F. Narita, F. Berto, Mixed mode fracture behavior of notched giant magnetostrictive: mechanical characterization and comparison among failure criteria, Theor. Appl. Fract. Mech. 99 (2019) 194–204.

[13] P. Taheri, R. Barua, J. Hsu, M. Zamanpour, Y. Chen, V.G. Harris, Structure, magnetism, and magnetostrictive properties of mechanically alloyed Fe81Ga19, J. Alloy. Compd. 661 (2016) 306–311.

[14] Z.X. Deng, M.J. Dapino, Magnetic flux biasing of magnetostrictive sensors, Smart Mater. Struct. 26 (2017), 055027.

[15] Z.X. Deng, M.J. Dapino, Review of magnetostrictive vibration energy harvesters, Smart Mater. Struct. 26 (2017), 103001.

[16] F. Narita, Inverse magnetostrictive effect in Fe29Co71 wire/polymer composites, Adv. Eng. Mater. 19 (2017), 1600586.

[17] L.B. Gao, H.T. Zhang, J.U. Surjadi, P.F. Li, Y. Han, D. Sun, Y. Lu, Mechanically stable ternary heterogeneous electrodes for energy storage and conversion, Nanoscale 10 (2018) 2613–2622.

[18] K. Katabira, Y. Yoshida, A. Masuda, A. Watanabe, F. Narita, Fabrication of Fe-Co magnetostrictive fiber reinforced plastic composites and their sensor performance evaluation, Materials 11 (2018) 406.

[19] Z.J. Yang, K. Nakajima, R. Onodera, T. Tayama, D. Chiba, F. Narita, Magnetostrictive clad steel plates for high-performance vibration energy harvesting, Appl. Phys. Lett. 112 (2018), 073902.

[20] Z. J. Yang, H. Kurita, H. Takeuchi, K. Katabira, F. Narita, Enhancement of inverse magnetostrictive effect through stress concentration for a notch-introduced FeCo alloy. Adv. Eng. Mater. (in press).

[21] F. Narita, M. Fox, A review on piezoelectric, magnetostrictive, and magnetoelectric materials and device technologies for energy harvesting applications, Adv. Eng. Mater. 20 (2018), 1700743.

[22] C.M. Leung, J.F. Li, D. Viehland, X. Zhuang, A review on applications of magnetoelectric composites: from heterostructural uncooled magnetic sensors, energy harvesters to highly efficient power converters, J. Phys. D-Appl. Phys. 51 (2018), 263002.

[23] Y. Wan, D. Fang, K.-C. Hwang, Non-linear constitutive relations for magnetostrictive materials, Int. J. Non-Linear Mech. 38 (2003) 1053–1065.

[24] F. Narita, K. Katabira, Stress-rate dependent output voltage for Fe29Co71 magnetostrictive fiber/polymer composites: fabrication, experimental observation and theoretical prediction, Mater. Trans. 58 (2017) 302–304.